Western University
Scholarship@Western

Chemistry Publications | Chemistry Department

3-20-2018

Crown Ether Effects on the Location of Charge Carriers in Electrospray Droplets: Implications for the Mechanism of Protein Charging and Supercharging.

Haidy Metwally

Lars Konermann

Follow this and additional works at: https://ir.lib.uwo.ca/chempub

Part of the Chemistry Commons

Citation of this paper:
Metwally, Haidy and Konermann, Lars, "Crown Ether Effects on the Location of Charge Carriers in Electrospray Droplets: Implications for the Mechanism of Protein Charging and Supercharging." (2018). *Chemistry Publications*. 252.
https://ir.lib.uwo.ca/chempub/252

Crown Ethers Modulate the Location of Charge Carriers in Electrospray Droplets: Implications for the Mechanism of Protein Charging and Supercharging

Haidy Metwally and Lars Konermann*

Department of Chemistry, The University of Western Ontario, London, Ontario, N6A 5B7, Canada

* corresponding author

E-mail address of the corresponding author: konerman@uwo.ca

Funding was provided by the Natural Sciences and Engineering Research Council of Canada (DG 217080-2013).

ABSTRACT: “Native” electrospray ionization (ESI) mass spectrometry (MS) aims to transfer proteins from solution into the gas phase while maintaining solution-like structures and interactions. The ability to control the charge states of protein ions produced in these experiments is of considerable importance. Supercharging agents (SCAs) such as sulfolane greatly elevate charge states without significantly affecting the protein structure in bulk aqueous solution. The origin of native ESI supercharging remains contentious. According to one model, SCAs trigger unfolding within ESI droplets. In contrast, the “charge trapping model” envisions that SCAs impede the ejection of charge carriers (e.g., NH_4^+ or Na^+) from the droplet. We addressed this controversy experimentally and computationally by employing 18C6 crown ether as a mechanistic probe in native ESI-MS experiments on holo-myoglobin. Remarkably, 18C6 suppressed the supercharging capability of sulfolane. Molecular dynamics (MD) simulations reproduced the experimental charge states. The MD data revealed that 18C6 altered the location of charge carriers in the ESI droplets. Without 18C6, sulfolane covered the droplets in an ionophobic layer that impeded charge carrier access to the surface. In contrast, 18C6 complexation caused charge carrier enrichment in this surface layer, thereby promoting charge ejection. For late droplets all the water had left and the protein was encapsulated in sulfolane; charge ejection at this stage continued only in the presence of 18C6. As a result, evaporation to dryness of charge-depleted water/sulfolane/18C6 droplets produced low protein charge states, whereas charge-abundant water/sulfolane droplets generated high charge states. Our data support the view that native ESI supercharging is caused by charge trapping. Unfolding within the droplet may play an ancillary role under some conditions, but for the cases examined here protein structural changes are not a causative factor for supercharging. Our conclusions are bolstered by dendrimer supercharging experiments.

Electrospray ionization (ESI)[1] transforms solution phase proteins into multiply charged gaseous ions for analysis by mass spectrometry (MS). Of particular interest are "native" ESI-MS experiments[2-4] that aim to preserve solution structures and interactions in the gas phase. These studies employ non-denaturing aqueous solutions and gentle ion sampling conditions. Native ESI-MS reports on protein binding stoichiometries.[2-5] Complementary information is obtainable from dissociation experiments[2, 6, 7] and ion mobility spectrometry.[8-10]

In positive ESI the protein solution is dispersed into droplets that carry excess H^+, NH_4^+, or Na^+.[11, 12] Evaporation and fission events close to the Rayleigh limit produce progressively smaller droplets.[11, 13] The mechanisms of analyte ion release from these nanodroplets were shrouded in controversy for many years.[1, 11, 12, 14-17] Recent molecular dynamics (MD) simulations helped address some of the questions in this area.[18-24] For example, it is now widely accepted that globular proteins are released via droplet evaporation to dryness during native ESI,[20-24] as envisioned by the charged residue model (CRM).[11, 25] Charge carriers bind to the protein during the final stages of evaporation, generating ions such as $[M + zH]^{z+}$ or $[M + zNa]^{z+}$.[11]

The dissociation behavior[26-32] and conformations of gaseous proteins[33-35] are governed by their charge state z. As a result, there is considerable interest in ways to manipulate these charge states.[33, 34, 36-39] Native ESI generates low z values close to the Rayleigh charge of protein-sized water droplets,[11, 25] in accordance with the CRM.[20-24] Much higher charge states are generated from proteins that are unfolded in bulk solution.[40, 41] According to the chain ejection model (CEM) these highly charged ions form during protein expulsion from the droplet surface.[42-44]

A common strategy for modulating protein charge states is the use of supercharging agents (SCAs).[45, 46] SCAs are added to the sample at low concentrations that do not significantly affect the protein structure in bulk solution.[44, 47] Yet, SCAs significantly enhance charging during ESI. Typical SCAs (such as sulfolane, $C_4H_8SO_2$) possess a nonpolar hydrocarbon moiety and one or

more polar groups.[32, 45, 47] Their low volatility makes them evaporate more slowly than water, such that late ESI nanodroplets are SCA-enriched.[32, 45, 47, 48] Supercharging takes place for native[30, 38, 45, 47, 49-53] and for denaturing solutions.[32, 44, 54] Here, we focus on the role of SCAs in native ESI, i.e., the conversion of folded solution phase proteins to highly charged gaseous ions.[30, 38, 45, 47, 49-52, 55]

The mechanism of native ESI supercharging remains controversial.[45, 46, 48, 50, 54, 56] According to one proposal supercharging is caused by thermal or chemical unfolding in SCA-enriched droplets.[47] Within this model, SCAs cause proteins to switch from the CRM to the CEM.[44] Although this "unfolding model" offers an intuitive explanation for supercharging, its validity is under dispute.[30, 45, 55, 57-59] The elevated CCSs observed for some supercharged proteins[44, 47, 58] do not prove that unfolding takes place within the droplet; alternatively, unfolding could be caused by Coulombic repulsion *after* release into the gas phase.[58, 60] A number of supercharged proteins retain a native-like compactness,[30, 60] making it unlikely that unfolding constitutes the root cause of supercharging. Also, weakly bound complexes can be supercharged without undergoing dissociation,[30, 45, 55] prompting, Robinson et al.[59] to conclude that "*supercharging does not appear to perturb the structure in that unfolding is not detected*".

Our group recently addressed this issue by applying MD simulations in which Na^+ served as excess charge carrier for probing the supercharging mechanism, focusing on the SCAs sulfolane and *m*-nitrobenzyl alcohol (*m*-NBA).[58] The MD-generated $[M + zNa]^{z+}$ ions closely matched the *z* values of experimentally observed sodiated and protonated protein ions, both with and without SCAs. In the simulations proteins were released via droplet evaporation to dryness. Droplet shrinkage was accompanied by charge carrier ejection. The remaining charge carriers underwent binding to the protein during the final stage of evaporation. The simulations indicated (i) SCA enrichment at the droplet surface, followed by (ii) formation of an SCA layer around the protein after complete water evaporation. Both factors inhibited charge carrier ejection from the droplet

because SCAs are ionophobic[58] (e.g., the NaCl solubility in sulfolane is four orders of magnitude lower than in water[61]). We thus proposed[58] that supercharging is caused by charge trapping, not by unfolding. This "charge trapping model"[58] and the aforementioned unfolding model[44, 47] represent two very different mechanistic views of protein supercharging in native ESI.

The current work examines the supercharging mechanism from a new perspective. Crown ethers can bind small cations, thereby enhancing the solubility of these charge carriers in nonaqueous solvents.[62, 63] We will test the following hypothesis: The charge trapping model[58] envisions that supercharging is caused by the low solubility of charge carriers in the SCA-enriched droplet layers. Under such conditions, the capability of crown ethers to act as phase transfer catalysts[62, 63] should facilitate the shuttling of charge carriers to the droplet surface, thereby favoring charge ejection. We predict that these conditions will lower the extent of protein charging in the presence of SCAs. 18-crown-6 (18C6) is of particular interest due to its ability to accommodate ESI-relevant species (Na^+, NH_4^+ and H_3O^+) in solution and in the gas phase.[62, 64-67] Previous studies explored 18C6 binding to Lys^+ and N^+-termini of gaseous peptides or proteins,[68-72] but the consequences of crown ethers for the ESI process remain largely unexplored.[39] The MD simulations of this work, as well as experiments on proteins and dendrimers, support the proposed hypothesis. We report for the first time that 18C6 acts as a powerful supercharging antidote. These findings support the view that native ESI supercharging is caused by charge trapping.

Materials and Methods

Protein ions were produced from neutral aqueous solutions by nanoESI using gold-coated borosilicate glass emitters at a flow rate of ~40 nL min^{-1}. Mass spectra were acquired on a Synapt instrument (Waters, Milford, MA). Gromacs 5[73] was used for MD simulations[24, 58] on various

droplets with an initial radius of 4 nm: (a) 8000 waters, (b) 7500 waters and 32 18C6, (c) 5300 waters and 460 sulfolane, (d) 4800 waters, 460 sulfolane, and 32 18C6. Simulations producing $[M + zH]^{z+}$ ions would require *ab initio* methods that are unsuitable for the system size and time scale studied here.[74] As in previous work,[35,70] our simulations thus used Na^+ as charge carriers, culminating in the formation of $[M + zNa]^{z+}$ instead of $[M + zH]^{z+}$.[11] Production runs were conducted at 370 K for 75 ns, followed by 200 ns at 450 K. Using standard MD, the slow evaporation of sulfolane and 18C6 would cause an unacceptable increase in wall clock time.[58] We thus subjected sulfolane and 18C6 to forced evaporation[58] starting at t = 150 ns. i.e., after the droplet had shrunk to a fraction of its initial size due to complete water loss. The forced evaporation algorithm is analogous to the use of a biasing potential, which represents a widely used strategy for accelerating MD simulations.[75-77] Complete details are found in the SI.

Results and Discussion

Effects of 18C6 on ESI Charge States. This work focused on holo-myoglobin (hMb), a heme-protein complex that served as model system for many earlier mechanistic studies.[38, 45, 47, 53, 58] Native ESI in aqueous ammonium acetate solution generated hMb ions in the 8+ and 9+ charge states (Figure 1a), very similar to earlier data recorded on different instruments and with different ESI sources.[40, 47, 58] Addition of 1 mM 18C6 resulted in crown ether adduction,[68] and a shift to slightly lower charge states (from 8+/9+ to 6+/7+, Figure 1b). Collisional activation caused loss of the 18C6 adducts, while the charge state distribution remained virtually unchanged (Figure 1d).

18C6 Suppresses Supercharging. Sulfolane is a typical SCA. As expected from earlier reports,[30, 32, 38, 44, 45, 47, 49-52, 54] high charge states (around 15+, Figure 1e) were observed when

electrospraying hMb from sulfolane-containing aqueous ammonium acetate. The supercharged protein ions largely retained their heme group,[45] whereas denaturation in solution usually disrupts heme-protein interactions.[40] Remarkably, the addition of 1 mM 18C6 to the sulfolane-containing solution suppressed supercharging, i.e., the hMb charge state distribution shifted from around 15+ into the 6+ to 9+ range (Figure 1f). The experiments were repeated with collisional activation (cone 120 V). Similar to the sulfolane-free solutions (Figure 1b, d), these harsher conditions removed 18C6 adducts without major changes of the charge state distribution (Figure 1f, h). It appears that the capability of 18C6 to act as supercharging antidote has not been reported before.

18C6 Effects in NaCl-Containing Solutions. Native ESI-MS experiments on hMb were repeated in solutions containing NaCl instead of ammonium acetate, giving rise to the formation of $[M + (z-n)H + nNa]^{z+}$ ions, all the way to fully sodiated $[M + zNa]^{z+}$.[11] These conditions resemble those used for the subsequent MD simulations, where Na^+ served as charge carrier. In addition to gentle ESI conditions, we tested the effects of source activation by raising the cone voltage. Alternatively, collisional activation was applied by raising the trap CE (Figure S2). All experiments were also repeated with ubiquitin, another common test protein (Figure S3).

The data obtained for the NaCl-containing samples resemble those of Figure 1 and can be summarized as follows: Sulfolane causes supercharging. Addition of 1 mM 18C6 to the sulfolane-containing solution shifts the spectra back to low charge states. This supercharging suppression was observed even when lowering the 18C6 concentration from 1 mM to 0.1 mM or 0.01 mM (Figure S4). Collisional activation removes 18C6 adducts without major charge states alterations. Thus, 18C6-induced shifts to lower charge states are *not* primarily caused by the loss of 18C6-bound charge carriers from the gaseous protein. This conclusion is consistent with previous work,[71] where it was noted that collisional charge loss (such as protein-NH_3^+···18C6 → protein-

NH_2 + $[18C6+H]^+$) is enthalpically unfavorable, in agreement with the data of Figure S1. Therefore, the capability of 18C6 to act as supercharging antidote must have a different origin. We resorted to MD simulations for uncovering the basis of this phenomenon.

Comparing MD and Experimental Results. The ESI droplets modeled here (initial radius 4 nm) were significantly larger than in earlier studies,[18-24] resembling the size regime encountered in experiments.[11] Charge states predicted by MD simulations on four types of hMb-containing droplets are compiled in Figure 2, along with the corresponding experimental data. Gratifyingly, the MD data reproduced the experimental trends. Water droplets produced charge states around 8+/9+. Slightly lower charge states were seen for water/18C6. Supercharged proteins with *z* values around 14+/15+ were produced from water/sulfolane droplets. The addition of 18C6 to the water/sulfolane droplets dramatically reduced the extent of protein charging. The subsequent MD trajectory analyses reveal the physical reasons underlying the sulfolane and 18C6 effects on protein ESI charge states.

The forced evaporation tool applied during the final stages of droplet shrinkage necessitated small corrections for MD charge states generated in the presence of 18C6 (see SI Methods). Figure 2 includes results obtained with and without this correction. The MD data reproduced the experimental trends, regardless whether the correction was applied or not.

Common Features of MD Trajectories. Snapshots taken from representative MD runs for the four conditions are summarized in Figure 3. All trajectories shared several features: The evaporating droplets retained an approximately spherical shape, with the protein in the interior. Multiply charged gaseous hMb was produced via solvent evaporation to dryness, as envisioned by the CRM.[20-24, 58] Droplet shrinkage was accompanied by Na^+ ejection from the droplet surface.

None of these IEM events[14, 18, 42] involved completely desolvated Na^+, instead the departing charge carriers were bound to 18C6 and/or several water or sulfolane molecules. Examples of such IEM events are highlighted in Figure 3. Ejected 18C6-bound charge carriers can be observed experimentally. Aqueous ammonium acetate/18C6 solution produced intense signals for $[18C6 + NH_4]^+$ and $[18C6 + Na]^+$ (Figure S5), underscoring the role of Na^+ as ubiquitous contaminant in analyte solutions,[11] and giving credence to the use of Na^+ in our simulations.[24, 58]

Principles that Govern the ESI Charge States of Proteins. Before proceeding, it is helpful to summarize the rules that govern the charge carrier behavior in native ESI.[24, 58] (i) Charge carriers can experience only two fates, ejection from the droplet or binding to the protein. (ii) The ejection of bare charge carriers from desolvated proteins is not feasible, at least not for the charge state range considered here.[78] (iii) Any charge carriers that are not ejected from the droplet will become part of the protein charge. (iv) Prerequisite for each charge ejection from the droplet is that the charge carrier can (at least transiently) reside close to the droplet surface; any factor that tends to exclude charge carriers from the surface will lower the charge ejection efficiency. From (i) - (iv) it follows that any factor that hinders charge carrier access to the droplet surface will increase the protein charge z. The repercussions of these considerations will become clear in the next section.

MD Trajectories Reveal the Basis of Charging and Supercharging. In *aqueous droplets* water and Na^+ shared the same radial distributions (Figure 4a), reflecting the favorable solvation of Na^+ in H_2O.[79] Under these conditions Na^+ can roam the entire solvent-occupied volume, including positions at the droplet surface from where charge ejection readily takes place (Figure 4b). As the final water molecules evaporated, charge ejection came to a halt (Figure 4b, c). The remaining Na^+ underwent irreversible binding to hMb (Figure 3a, $t \approx 92$ ns) at protein carboxylates (Figure S6).

For *water/18C6 droplets* (Figure 3b) all 18C6 were located close to the droplet surface, consistent with their amphiphilic nature.[62, 63, 80-82] Na^+ exhibited a bimodal radial distribution, comprising water-solvated Na^+ in the droplet interior and $[18C6 + Na]^+$ at the droplet surface (Figure 4d). The positioning of $[18C6 + Na]^+$ at the liquid/vapor interface facilitated ejection of these complexes from the droplet. Thus, the high surface affinity of $[18C6 + Na]^+$ was responsible for the slightly lower protein charge states in water/18C6 compared to pure water (Figure 2). The behavior seen here for $[18C6 + Na]^+$ mirrors the facile IEM ejection of other cationic solutes that carry nonpolar groups.[12] Charge ejection ceased just prior to evaporation of the last water molecules (Figure 4e,f). At this point, residual Na^+ and $[18C6 + Na]^+$ underwent ion pairing with protein carboxylates, while non-sodiated 18C6 bound to Lys^+ (Figure S6).[68-72] These MD-predicted 18C6 adducts were experimentally observable under gentle ESI conditions (Figure 1b). The number of MD-adducted 18C6 (10 ± 1) was consistent with the experimental data of Figure 1b, where the most intense signal corresponded to hMb^{6+} attached to 10 crown ethers. 18C6 removal by MD forced evaporation (Figures 3b, 4e) or by collisional heating (Figure 1d) produced fully desolvated hMb.

Water/sulfolane droplets (Figure 3c) showed sulfolane enrichment in the outermost layers. This nanoscale segregation is consistent with phenomena reported for other binary mixtures, such as methanol/water or ethanol/water, where the nonaqueous component undergoes surface enrichment despite being "fully miscible" in bulk solution.[80-83] A key driving force for the sulfolane/water segregation seen here is the maximization of enthalpically favorable water-water contacts in the droplet core.[84] (Analogous arguments explain why 18C6 is driven to the surface of the water/18C6 droplets discussed in the preceding paragraph.[80-84]) For the ESI water/sulfolane droplets of Figure 3c these segregation phenomena produced a sulfolane-enriched surface layer that surrounded the protein-containing aqueous core (Figure 4g). The ionophobic nature of

sulfolane[58, 61] (along with the high water affinity of Na^+)[79] largely confined the charge carriers to the droplet interior. The resulting Na^+ depletion at the droplet surface reduced the charge ejection probability. Because of this reduced IEM efficiency, a larger number of Na^+ remained trapped within the droplet compared to the water or water/18C6 droplets (Figures 4h vs. 4b, 4e). Complete H_2O loss from the water/sulfolane droplets subsequently generated sulfolane-encapsulated hMb, concomitant with irreversible binding of all remaining Na^+ to protein carboxylates (Figure 3c, t = 92 ns). Further charge loss would require the occurrence of highly unfavorable events, i.e., dissociation of protein-$COO^-\cdots Na^+$ ion pairs, followed by Na^+ diffusion through the ionophobic sulfolane environment. Hence, the protein attained its final "supercharged" z value after all water had left the droplet, but long before evaporation of the sulfolane shell had gone to completion.

These data for water/sulfolane reflect the charge trapping model outlined in the Introduction.[58] This mechanism causes supercharging via two interrelated factors, i.e., (i) formation of a SCA layer at the droplet surface that tends to confine charges to the aqueous interior, thereby impeding charge ejection. (ii) After complete water loss, the protein becomes surrounded by an SCA shell and the remaining charge carriers are forced to associate with protein carboxylates. Charge partitioning during droplet shrinkage is governed by the *low* affinity of charge carriers for the SCA, their *greater* affinity for protein carboxylates, and their *high* affinity for water[58, 79] For the three droplet types discussed so far (water, water/18C6, water sulfolane), only Na^+ solvation by water prevented irreversible charge carrier binding to the protein. Charge ejection came to a halt once the number of H_2O dropped below ~200 (vertical lines in Figure 4b, e, h), forcing freely diffusible Na^+_{aq} to transition into carboxylate-bound environments.

As noted, a key element of the charge trapping model is that SCAs exhibit a low charge carrier affinity. This aspect is consistent with earlier work that focused on protein charging by H^+, where it was noted that SCAs generally exhibit a low H^+ affinity in solution (i.e., a weak Brønsted

basicity).[48, 85] These parallels support the view that the charge trapping model is not limited to droplets containing Na^+, but that it also applies to H^+ and other ESI-relevant charge carriers.

In *water/sulfolane/18C6 droplets* the charge carriers exhibited a bimodal distribution, with H_2O-solvated Na^+ in the interior and abundant sulfolane-solvated $[18C6 + Na]^+$ in the outermost droplet layers (Figure 4j). The latter reflect the capability of crown ethers to solubilize cations in unfavorable solvents.[62, 63] $[18C6 + Na]^+$ enrichment at the droplet surface facilitated the ejection of these charged complexes. Numerous $[18C6 + Na]^+$ remained at the surface of the droplet even after complete water evaporation, thereby ensuring *continued* charge ejection and suppression of charge carrier binding to the protein (Figure 3d at t = 92 ns, Figure 4k, l). In summary, the MD data reveal that 18C6 nullifies the charge-enhancing effects of the SCA by eliminating charge trapping. Our results confirm the hypothesis stated in the Introduction, i.e., the proposal that 18C6 binds charge carriers (Na^+, NH_4^+, H_3O^+)[62, 64-67] and shuttles them through the SCA trapping layer.

Relationship between Supercharging and Unfolding. Our MD runs showed that hMb in water/sulfolane retained a compact structure until the droplet had almost completely dried out (Figure 3c), long after the final z value had been attained via Na^+ binding. Coulombically driven unfolding of the supercharged protein started to take place during the final solvent evaporation steps (Figure S7). Hence, for the conditions examined here, unfolding is caused by supercharging and not *vice versa*. In other words, our data argue against the idea that native ESI supercharging is caused by protein unfolding within the droplet, with subsequent protein extrusion from the droplet surface.[44, 47] Instead, our findings support the view that supercharging is caused by charge trapping. While supercharged hMb undergoes unfolding in the gas phase,[47, 58] other supercharged proteins are more resilient and retain native-like properties.[30, 45, 55, 60] The experimental observation

of such compact supercharged proteins[30, 45, 55, 60] would be difficult to reconcile with the unfolding model,[44, 47] while our charge trapping model readily explains how such species can form.

Notwithstanding the aforementioned conclusions, we do not rule out that unfolding may contribute to supercharging under some conditions, likely in combination with the SCA-mediated charge trapping outlined above. The latter scenario is supported by data on disulfide intact and reduced proteins.[44] The possible occurrence of protein unfolding within the droplet will depend on various factors, including the droplet lifetime,[86] confinement effects,[87] and interactions with gas/liquid interfaces.[88]

Dendrimer Supercharging. Dendrimers are hyperbranched globular macromolecules that are incapable of large-scale unfolding.[89, 90] These analytes are well suited for further scrutinizing the competing supercharging models. The charge trapping model predicts that dendrimers will undergo supercharging, while according to the unfolding model dendrimers should be immune to SCAs.[44, 47] For meaningful test experiments it is important to use dendrimers with ”protein-like” properties, i.e., with both acidic and basic sites, and with a MW similar to that of typical proteins.

Earlier work[46] examined the behavior of DAB-16 (1687 Da) and DAB-64 dendrimers (7168 Da). The former did not undergo supercharging. For the latter, the presence of SCA in water caused a broadened charge state distribution that suggested supercharging for a sub-population of the analytes. The implications of those data[46] for proteins are inconclusive The absence of carboxylates in DAB dendrimers prevents analyte charging via $R\text{-}COO^-$ neutralization, unlike for proteins where carboxylates represent the main charge carrier binding sites.[24] In addition, the small size of DAB-16 raises questions as to whether this species exhibits true CRM behavior.[1]

Here we tested the behavior of G5 PAMAM succinamic acid dendrimer. Its theoretical MW (41669 Da) is comparable to proteins that have previously been subjected to native ESI

supercharging.[30, 45, 55, 59, 60] This dendrimer possesses both basic sites (tertiary amines) and acidic moieties (succinamic acid groups). A slight complication is the fact that PAMAM dendrimers generally exhibit mass heterogeneity arising from defects in their branched structures, particularly for large species that are comparable in size to proteins.[90] ESI mass spectra recorded in aqueous solution showed several broad maxima that can be attributed to the charge state range of 7+ to 12+ (Figure 5a). Upon addition of sulfolane the spectra underwent a dramatic shift towards lower *m/z*, corresponding to charge states around 15+ and higher (Figure 5b). Similar data were obtained when repeating the experiments in NaCl-containing solution (Figure S8). These spectra demonstrate the occurrence of sulfolane-induced supercharging for the PAMAM dendrimer, confirming the prediction of the charge trapping model.

Conclusions

The current work demonstrates that MD simulations represent a powerful tool for probing the behavior of ESI droplets containing multiple interacting components. We applied crown ethers as a mechanistic probe of the ESI process. The ability of 18C6 to act as phase transfer catalyst[62, 63] alters the location of charge carriers inside ESI droplets, with dramatic consequences for protein charge states. Crown ethers may also influence protein structures in solution[91, 92] and in the gas phase,[70] but our data do not support the view that such conformational factors are responsible for the charge state shifts reported here. The mechanistic insights obtained in the current work can be summarized in cartoon form (Figure 6), where blue "+" symbols indicate charge carriers. While the current work focused on Na^+, Figures 1, S2, S3 suggest that similar considerations also apply to other ESI-relevant charge carriers such as H_3O^+ and NH_4^+.[11, 85]

Evaporating ESI nanodroplets experience internal Coulomb repulsion which tends to trigger charge ejection via the IEM.[17] The efficiency of these events is modulated by the capability of charge carriers to migrate to the droplet surface (because only *surface* charges can undergo IEM ejection[12, 14]). In aqueous solution (Figure 6a) the favorable solvation characteristics afforded by water allow charge carriers to adopt positions throughout the droplet, including locations close to the surface from where they can be ejected. The relatively few remaining charge carriers in the vanishing droplet bind to the protein, producing low CRM charge states.[11, 24, 25]

The addition of SCA leads to supercharging via charge trapping (Figure 6b).[58] The SCA initially forms an ionophobic surface layer. As a result, charge carriers preferentially reside in the droplet interior such that their IEM efficiency is reduced; thus, a larger number of charge carriers remain in the droplet compared to the purely aqueous droplets. Once all the water has evaporated the SCA encapsulates the protein. Unfavorable interactions with the SCA force the remaining charge carriers to associate with the protein. All these (many) charge carriers remain bound until the SCA layer has evaporated – producing a desolvated supercharged protein ion. Depending on their structural resilience, supercharged proteins may undergo electrostatically driven unfolding (as in the case of hMb[47, 58]), or they can retain compact conformations (as demonstrated for several other proteins[30, 45, 55, 59, 60]). Our MD simulations and dendrimer supercharging data do not support the view that unfolding within the ESI droplet is the root cause of supercharging.[44, 47]

Figure 6c illustrates how 18C6 acts as supercharging antidote. 18C6 solubilizes charge carriers in the SCA, allowing the charge carriers to reside at the droplet surface such that IEM ejection proceeds with high efficiency. Compared to the supercharging conditions of Figure 6b the droplets lose more charge, such that the dried-out protein at the end of the process has a lower *z*.

Experimental supercharging spectra exhibit wide charge state distributions (Figure 1e, g), whereas our simulations produced fairly well defined *z* values (Figure 2). The experimentally

observed charge state range is attributed to the heterogeneous nature of evaporation/fission events in the ESI plume, which will yield nanodroplets with different SCA concentrations.[11] Nanodroplets containing more SCA will produce higher *z* values.[47, 58] Modeling this heterogeneity is difficult, as it would require knowledge of the exact ESI plume composition. Regardless of these nuances, it is remarkable how well the current MD data capture the experimental trends, i.e., a dramatic shift to higher charge states in the presence of sulfolane and the suppression of supercharging by 18C6 (Figure 2).

Our use of 18C6 as a mechanistic ESI probe expands on previous studies, where this remarkable molecule was applied to examine protein structures in solution[68] and in the gas phase.[69, 70] In future work we hope to apply strategies similar to those used here for uncovering the mechanistic basis of supercharging under denaturing conditions, where the charge states formed are even higher than under the native ESI conditions examined here.[32, 44, 54]

Supporting Information Available. Complete Methods and additional figures as noted in the text. This material is available free of charge via the Internet at http://pubs.acs.org.

Acknowledgements. We thank Angela Murcia-Rios, Victor Yin, and Elizabeth Gillies for helpful discussions.

References

(1) Nguyen, S.; Fenn, J. B. *Proc. Natl. Acad. Sci. U.S.A.* **2007**, *104*, 1111-1117.
(2) Marty, M. T.; Zhang, H.; Cui, W. D.; Blankenship, R. E.; Gross, M. L.; Sligar, S. G. *Anal. Chem.* **2012**, *84*, 8957-8960.
(3) Leney, A. C.; Heck, A. J. R. *J. Am. Soc. Mass Spectrom.* **2017**, *28*, 5-13.
(4) Marcoux, J.; Robinson, C. V. *Structure* **2013**, *21*, 1541-1550.
(5) Daniel, J. M.; Friess, S. D.; Rajagopalan, S.; Wendt, S.; Zenobi, R. *Int. J. Mass Spectrom.* **2002**, *216*, 1-27.
(6) Bonner, J. G.; Lyon, Y. A.; Nellessen, C.; Julian, R. R. *J. Am. Chem. Soc.* **2017**, *139*, 10286-10293.
(7) Han, L.; Hyung, S.-J.; Mayers, J. J. S.; Ruotolo, B. T. *J. Am. Chem. Soc.* **2011**, *133*, 11358-11367.
(8) El-Baba, T. J.; Woodall, D. W.; Raab, S. A.; Fuller, D. R.; Laganowsky, A.; Russell, D. H.; Clemmer, D. E. *J. Am. Chem. Soc.* **2017**, *139*, 6306-6309.
(9) Wyttenbach, T.; Bleiholder, C.; Bowers, M. T. *Anal. Chem.* **2013**, *85*, 2191-2199.
(10) Marklund, E. G.; Degiacomi, M. T.; Robinson, C. V.; Baldwin, A. J.; Benesch, J. L. P. *Structure* **2015**, *23*, 791-799.
(11) Kebarle, P.; Verkerk, U. H. *Mass Spectrom. Rev.* **2009**, *28*, 898-917.
(12) Cech, N. B.; Enke, C. G. *Mass Spectrom. Rev.* **2001**, *20*, 362-387.
(13) Grimm, R. L.; Beauchamp, J. L. *J. Phys. Chem. A* **2010**, *114*, 1411-1419.
(14) Iribarne, J. V.; Thomson, B. A. *J. Chem. Phys.* **1976**, *64*, 2287-2294.
(15) Cole, R. B. *J. Mass. Spectrom.* **2000**, *35*, 763-772.
(16) Loscertales, I. G.; de la Mora, J. F. *J. Chem. Phys.* **1995**, *103*, 5041-5060.
(17) Hogan, C. J.; Carroll, J. A.; Rohrs, H. W.; Biswas, P.; Gross, M. L. *Anal. Chem.* **2009**, *81*, 369-377.
(18) Znamenskiy, V.; Marginean, I.; Vertes, A. *J. Phys. Chem. A* **2003**, *107*, 7406-7412.
(19) Steinberg, M. Z.; Breuker, K.; Elber, R.; Gerber, R. B. *Phys. Chem. Chem. Phys.* **2007**, *9*, 4690-4697.
(20) Patriksson, A.; Marklund, E.; van der Spoel, D. *Biochemistry* **2007**, *46*, 933-945.
(21) Oh, M. I.; Consta, S. *J. Am. Soc. Mass Spectrom.* **2017**, *28*, 2262-2279.
(22) Kim, D.; Wagner, N.; Wooding, K.; Clemmer, D. E.; Russell, D. H. *J. Am. Chem. Soc.* **2017**, *139*, 2981-2988.
(23) Porrini, M.; Rosu, F.; Rabin, C.; Darre, L.; Gomez, H.; Orozco, M.; Gabelica, V. *ACS Central Sci.* **2017**, *3*, 454–461.
(24) McAllister, R. G.; Metwally, H.; Sun, Y.; Konermann, L. *J. Am. Chem. Soc.* **2015**, *137*, 12667-12676.
(25) de la Mora, F. J. *Anal. Chim. Acta* **2000**, *406*, 93-104.
(26) Siuti, N.; Kelleher, N. L. *Nat. Methods* **2007**, *4*, 817-821.
(27) Zubarev, R. A. *Mass Spectrom. Rev.* **2003**, *22*, 57-77.
(28) Syka, J. E. P.; Coon, J. J.; Schroeder, M. J.; Shabanowitz, J.; Hunt, D. F. *Proc. Natl. Acad. Sci. U.S.A.* **2004**, *101*, 9528-9533.
(29) Quintyn, R. S.; Zhou, M.; Yan, J.; Wysocki, V. H. *Anal. Chem.* **2015**, *87*, 11879-11886.
(30) Hall, Z.; Politis, A.; Bush, M. F.; Smith, L. J.; Robinson, C. V. *J. Am. Chem. Soc.* **2012**, *134*, 3429-3438.
(31) Zhang, J.; Loo, R. R. O.; Loo, J. A. *Int. J. Mass Spectrom.* **2015**, *377*, 546-556.
(32) Teo, C. A.; Donald, W. A. *Anal. Chem.* **2014**, *86*, 4455-4462.

(33) Shelimov, K. B.; Jarrold, M. F. *J. Am. Chem. Soc.* **1997**, *119*, 2987-2994.
(34) Laszlo, K. J.; Munger, E. B.; Bush, M. F. *J. Am. Chem. Soc.* **2016**, *138*, 9581-9588.
(35) Florez, A. I. G.; Mucha, E.; Ahn, D. S.; Gewinner, S.; Schollkopf, W.; Pagel, K.; von Helden, G. *Angew. Chem.-Int. Edit.* **2016**, *55*, 3295-3299.
(36) Jhingree, J. R.; Bellina, B.; Pacholarz, K. J.; Barran, P. E. *J. Am. Soc. Mass Spectrom.* **2017**, *28*, 1450-1461.
(37) Lermyte, F.; Williams, J. P.; Brown, J. M.; Martin, E. M.; Sobott, F. *J. Am. Soc. Mass Spectrom.* **2015**, *26*, 1068-1076.
(38) Fisher, C. M.; Kharlamova, A.; McLuckey, S. A. *Anal. Chem.* **2014**, *86*, 4581-4588.
(39) Pagel, K.; Hyung, S.-J.; Ruotolo, B. T.; Robinson, C. V. *Anal. Chem.* **2010**, *82*, 5363-5372.
(40) Dobo, A.; Kaltashov, I. A. *Anal. Chem.* **2001**, *73*, 4763-4773.
(41) Natalello, A.; Santambrogio, C.; Grandori, R. *J. Am. Soc. Mass Spectrom.* **2017**, *28*, 21-28.
(42) Konermann, L.; Ahadi, E.; Rodriguez, A. D.; Vahidi, S. *Anal. Chem.* **2013**, *85*, 2-9.
(43) Mehmood, S.; Allison, T. M.; Robinson, C. V. *Annu. Rev. Phys. Chem.* **2015**, *66*, 453-474.
(44) Donor, M. T.; Ewing, S. A.; Zenaidee, M. A.; Donald, W. A.; Prell, J. S. *Anal. Chem.* **2017**, *89*, 5107-5114.
(45) Lomeli, S. H.; Peng, I. X.; Yin, S.; Ogorzalek Loo, R. R.; Loo, J. A. *J. Am. Soc. Mass Spectrom.* **2010**, *21*, 127-131.
(46) Iavarone, A. T.; Williams, E. R. *J. Am. Chem. Soc.* **2003**, *125*, 2319-2327.
(47) Sterling, H. J.; Daly, M. P.; Feld, G. K.; Thoren, K. L.; Kintzer, A. F.; Krantz, B. A.; Williams, E. R. *J. Am. Soc. Mass Spectrom.* **2010**, *21*, 1762-1774.
(48) Ogorzalek Loo, R. R.; Lakshmanan, R.; Loo, J. A. *J. Am. Soc. Mass Spectrom.* **2014**, *25*, 1675-1693.
(49) Hogan, C. J.; Ogorzalek Loo, R. R.; Loo, J. A.; de la Mora, J. F. *Phys. Chem. Chem. Phys.* **2010**, *12*, 13476-13483.
(50) Chingin, K.; Xu, N. C., H. *J. Am. Soc. Mass Spectrom.* **2014**, *25*, 928-934.
(51) Zhou, M.; Dagan, S.; Wysocki, V. H. *Analyst* **2013**, *138*, 1353-1362.
(52) Ferguson, C. N.; Benchaar, S. A.; Miao, Z. X.; Loo, J. A.; Chen, H. *Anal. Chem.* **2011**, *83*, 6468-6473.
(53) Wang, H.; Yong, G.; Brown, S. L.; Lee, H. E.; Zenaidee, M. A.; Supuran, C. T.; Donald, W. A. *Anal. Chim. Acta* **2018**, *1003*, 1-9.
(54) Douglass, K. A.; Venter, A. R. *J. Am. Soc. Mass Spectrom.* **2012**, *23*, 489-497.
(55) Lomeli, S. H.; Yin, S.; Loo, R. R. O.; Loo, J. A. *J. Am. Soc. Mass Spectrom.* **2009**, *20*, 593-596.
(56) Samalikova, M.; Grandori, R. *J. Mass Spectrom.* **2005**, *40*, 503-510.
(57) Yao, Y.; Richards, M. R.; Kitova, E. N.; Klassen, J. S. *J. Am. Soc. Mass Spectrom.* **2016**, *27*, 498-506.
(58) Metwally, H.; McAllister, R. G.; Popa, V.; Konermann, L. *Anal. Chem.* **2016**, *88*, 5345-5354.
(59) Hall, Z.; Robinson, C. V. *J. Am. Soc. Mass Spectrom.* **2012**, *23*, 1161-1168.
(60) Sterling, H. J.; Kintzer, A. F.; Feld, G. K.; Cassou, C. A.; Krantz, B. A.; Williams, E. R. *J. Am. Soc. Mass Spectrom.* **2012**, *23*, 191-200.
(61) Burgess, J. *Metal Ions in Solution*; Ellis Horwood: New York, 1978.
(62) Pedersen, C. J. *J. Am. Chem. Soc.* **1967**, *89*, 7017-&.
(63) Landini, D.; Montanar.F; Pirisi, F. M. *J. Chem. Soc.-Chem. Commun.* **1974**, 879-880.
(64) Armentrout, P. B. *Int. J. Mass Spectrom.* **1999**, *193*, 227-240.
(65) Cram, D. J.; Cram, J. M. *Accounts Chem. Res.* **1978**, *11*, 8-14.

(66) Hurtado, P.; Gamez, F.; Hamad, S.; Martinez-Haya, B.; Steill, J. D.; Oomens, J. *J. Phys. Chem. A* **2011**, *115*, 7275-7282.
(67) Igumnov, S. N.; Mamontov, M. N.; Uspenskaya, I. A. *J. Chem. Eng. Data* **2012**, *57*, 456-461.
(68) Ly, T.; Julian, R. R. *J. Am. Soc. Mass Spectrom.* **2006**, *17*, 1209-1215.
(69) Bonner, J. G.; Hendricks, N. G.; Julian, R. R. *J. Am. Soc. Mass Spectrom.* **2016**, *27*, 1661-1669.
(70) Warnke, S.; von Helden, G.; Pagel, K. *J. Am. Chem. Soc.* **2013**, *135*, 1177-1180.
(71) Chen, Y.; Rodgers, M. T. *J. Am. Chem. Soc.* **2012**, *134*, 5863-5875.
(72) Stedwell, C. N.; Galindo, J. F.; Gulyuz, K.; Roitberg, A. E.; Polfer, N. C. *J. Phys. Chem. A* **2013**, *117*, 1181-1188.
(73) Abraham, M. J.; Murtola, T.; Schulz, R.; Páll, S.; Smith, J. C.; Hess, B.; Lindahl, E. *SoftwareX* **2015**, *1–2*, 19-25.
(74) Chen, M.; Ko, H. Y.; Remsing, R. C.; Andrade, M. F. C.; Santra, B.; Sun, Z. R.; Selloni, A.; Car, R.; Klein, M. L.; Perdew, J. P.; Wu, X. F. *Proc. Natl. Acad. Sci. U. S. A.* **2017**, *114*, 10846-10851.
(75) Nam, K.; Pu, J. Z.; Karplus, M. *Proc. Natl. Acad. Sci. U.S.A.* **2014**, *111*, 17851-17856.
(76) Lemkul, J. A.; Bevan, D. R. *J. Phys. Chem. B* **2010**, *114*, 1652-1660.
(77) Han, W.; Schulten, K. *J. Am. Chem. Soc.* **2014**, *136*, 12450-12460.
(78) Zenaidee, M. A.; Leeming, M. G.; Zhang, F. T.; Funston, T. T.; Donald, W. A. *Angew. Chem.-Int. Edit.* **2017**, *56*, 8522-8526.
(79) Mahler, J.; Persson, I. *Inorg. Chem.* **2012**, *51*, 425-438.
(80) Li, Z. X.; Lu, J. R.; Styrkas, D. A.; Thomas, R. K.; Rennie, A. R.; Penfold, J. *Mol. Phys.* **1993**, *80*, 925-939.
(81) Tarek, M.; Tobias, D. J.; Klein, M. L. *J. Chem. Soc.-Faraday Trans.* **1996**, *92*, 559-563.
(82) Raina, G.; Kulkarni, G. U.; Rao, C. N. R. *J. Phys. Chem. A* **2001**, *105*, 10204-10207.
(83) Dixit, S.; Crain, J.; Poon, W. C. K.; Finney, J. L.; Soper, A. K. *Nature* **2002**, *416*, 829-832.
(84) Brini, E.; Fennell, C. J.; Fernandez-Serra, M.; Hribar-Lee, B.; Luksic, M.; Dill, K. A. *Chem. Rev.* **2017**, *117*, 12385-12414.
(85) Nshanian, M.; Lakshmanan, R.; Chen, H.; Ogorzalek Loo, R. R.; Loo, J. A. *Int. J. Mass Spectrom.* **2018**, *(in press)*.
(86) Hamdy, O. M.; Julian, R. R. *J. Am. Soc. Mass Spectrom.* **2012**, *23*, 1-6.
(87) Zhou, H. X.; Rivas, G. N.; Minton, A. P. *Annu. Rev. Biophys.* **2008**, *37*, 375-397.
(88) Hedges, J. B.; Vahidi, S.; Yue, X.; Konermann, L. *Anal. Chem.* **2013**, *85*, 6469-6476.
(89) Boas, U.; Heegaard, P. M. H. *Chem. Soc. Rev.* **2004**, *33*, 43-63.
(90) Mintzer, M. A.; Grinstaff, M. W. *Chem. Soc. Rev.* **2011**, *40*, 173-190.
(91) Suzumura, A.; Paul, D.; Sugimoto, H.; Shinoda, S.; Julian, R. R.; Beauchamp, J. L.; Teraoka, J.; Tsukube, H. *Inorganic Chemistry* **2005**, *44*, 904-910.
(92) Lee, C. C.; Maestre-Reyna, M.; Hsu, K. C.; Wang, H. C.; Liu, C. I.; Jeng, W. Y.; Lin, L. L.; Wood, R.; Chou, C. C.; Yang, J. M.; Wang, A. H. J. *Angew. Chem.-Int. Edit.* **2014**, *53*, 13054-13058.

Figure Captions

Figure 1. Mass spectra acquired after electrospraying holo-myoglobin without (panels on left) and with 1 mM 18C6 (panels on right) in neutral aqueous solution containing 1 mM ammonium acetate. (a, b) Data recorded without sulfolane under gentle conditions, i.e., cone 20 V. Extensive adduct formation in (b) is due to noncovalent attachment of up to ~14 18C6. (c, d) Same as in (a) and (b), but with in-source activation (cone 100 V). (e, f) Spectra acquired after addition of 1% sulfolane under gentle conditions (cone 20 V). (g, h) Same as in (e) and (f), but with in-source activation (cone 120 V). h8+, a14+, etc. denote hMb and aMb charge states. * indicates free heme; # refers to an unidentified cluster.

Figure 2. ESI charge states of hMb obtained experimentally and from MD simulations. Experimental values are averages of three measurements acquired under the conditions of Figure 1 (cone 100 V, trap CE 4 V). MD data are based on five replicate runs for each condition. MD data for 18C6-containing droplets are shown with and without forced evaporation correction. Error bars represent standard deviations.

Figure 3. Snapshots taken from MD trajectories that culminate in the production of desolvated hMb ions from ESI nanodroplets. Four solvent conditions were tested: (a) water, (b) water/18C6, (c) water/sulfolane, (d) water/sulfolane/18C6. Time points are indicated along the left hand side. Charge states of protein ions at the end of the simulation runs are shown (at t = 275 ns). IEM ejection events of solvated and/or 18C6-complexed Na^+ are highlighted. Coloring: Protein, pink; heme, black; Na^+, blue; water oxygen, red; sulfolane, dark green; 18C6, orange/red.

Figure 4. MD data for four types of hMb-containing ESI droplets, as noted along the top. Top row: Spatial distribution of solutes, averaged over t = 25 to t = 32 ns in all repeat runs. For 18C6-containing droplets two separate Na^+ distributions are shown, reflecting the behavior of sodium in $[18C6 + Na]^+$ vs. all other sodium ions (denoted as Na^+_{free}). Middle and bottom rows: Time-dependent changes in droplet composition for four typical trajectories, reflecting the occurrence of solvent evaporation and charge ejection. Dashed vertical lines indicate the point where 200 water molecules remain in the droplet; after this point only panel (k) shows Na^+ ejection (as $[18C6 + Na]^+$). Dotted blue lines indicate Na^+ data after correction for $[18C6 + Na]^+$ forced evaporation (see SI Methods). The coloring of droplet components matches that of Figure 3.

Figure 5. ESI mass spectra of G5 PAMAM dendrimer in aqueous solution containing ammonium acetate (a) without sulfolane, (b) with sulfolane. Mass heterogeneity obscures individual charge states. Red lines indicate expected peak positions for the calculated theoretical mass.

Figure 6. Cartoon summary of MD and experimental results. (a) Native ESI in aqueous solution, producing low charge states. A similar scenario is encountered for water/18C6 droplets (not shown). (b) Supercharging via the charge trapping. A highly charged protein is formed because charge ejection from the droplet is hindered. The supercharged protein may undergo gas phase unfolding. (c) 18C6 acts as supercharging antidote; it prevents charge trapping by promoting the ejection of charge carriers from the droplet surface. "X^+" represents charge carriers such as Na^+, H_3O^+ or NH_4^+. "IEM" indicates charge carrier ejection (field emission).

Figure 1

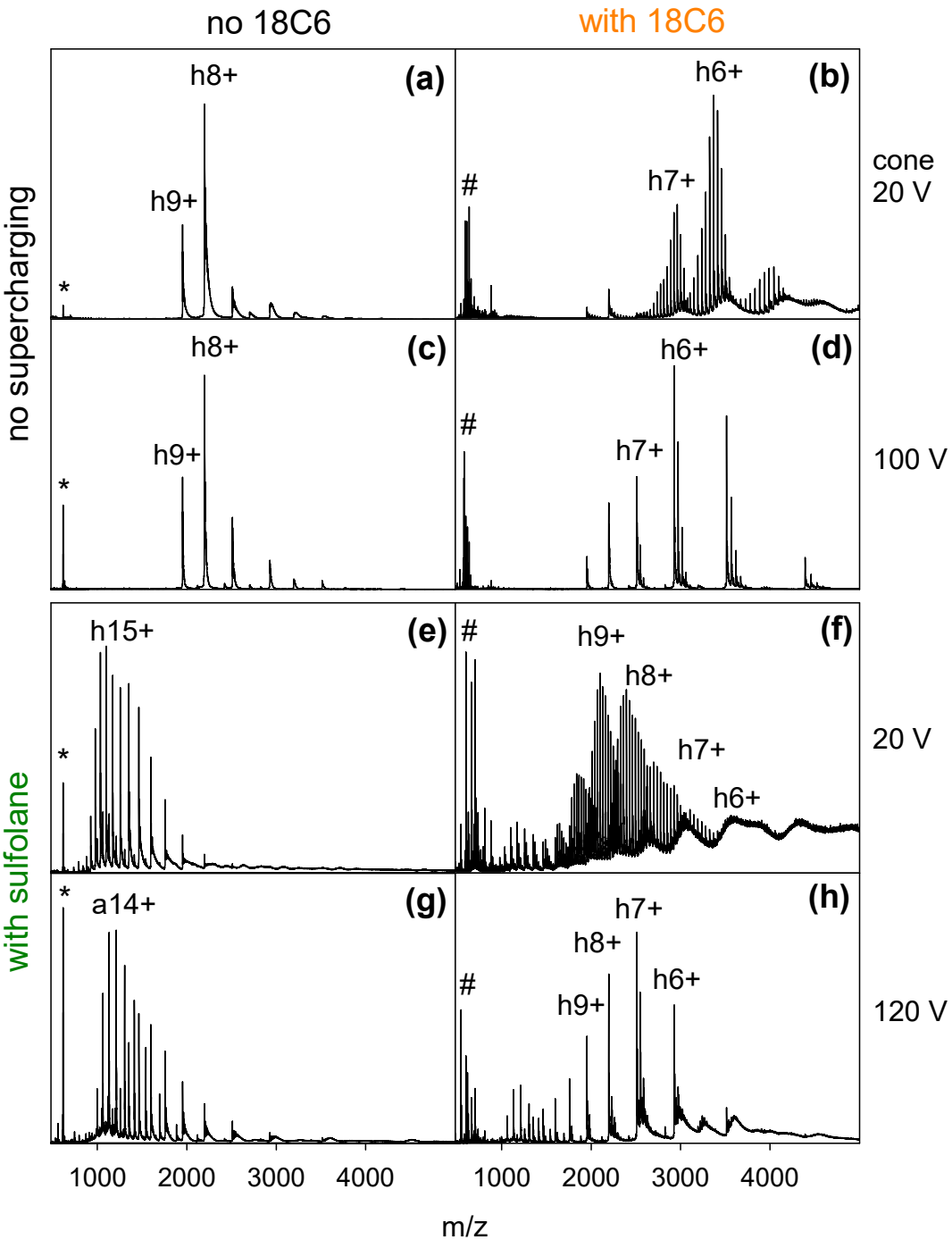
no 18C6
with 18C6
no supercharging
with sulfolane
cone 20 V
100 V
20 V
120 V
(a)
(b)
(c)
(d)
(e)
(f)
(g)
(h)
h8+
h9+
h6+
h7+
h15+
a14+
*
#
1000
2000
3000
4000
m/z

Figure 2

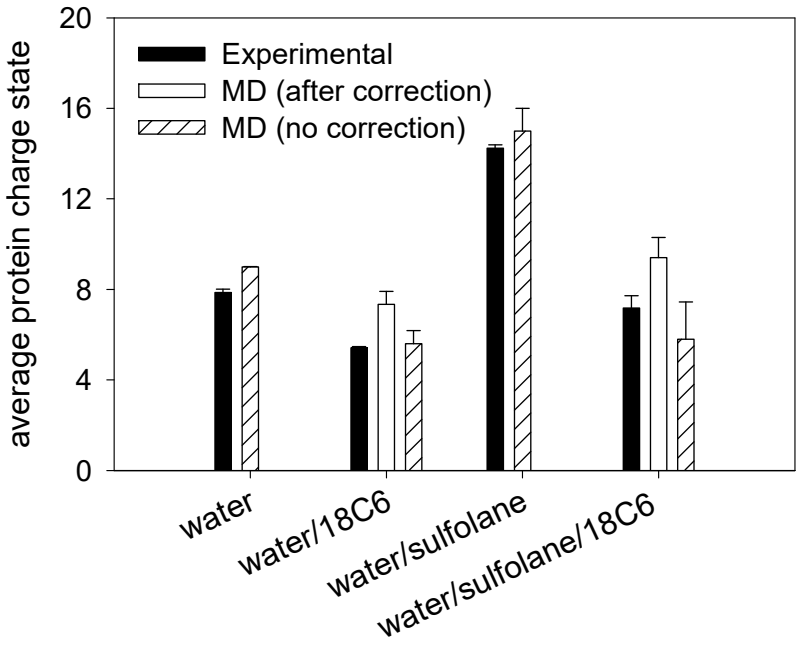
average protein charge state
20
16
12
8
4
0
Experimental
MD (after correction)
MD (no correction)
water
water/18C6
water/sulfolane
water/sulfolane/18C6

Figure 3

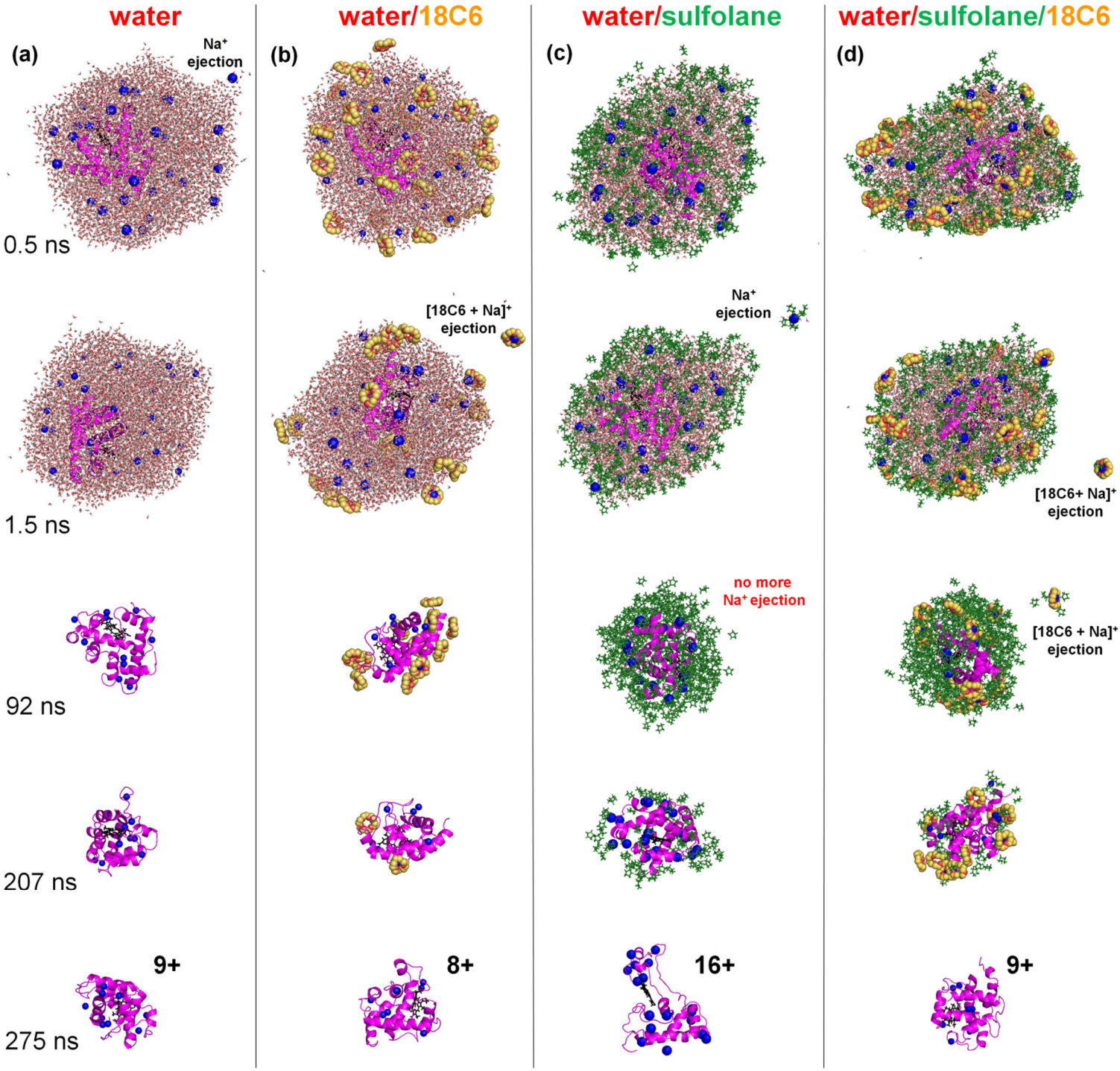
water
water/18C6
water/sulfolane
water/sulfolane/18C6
(a)
(b)
(c)
(d)
Na+ ejection
0.5 ns
[18C6 + Na]+ ejection
Na+ ejection
[18C6+ Na]+ ejection
1.5 ns
no more Na+ ejection
[18C6 + Na]+ ejection
92 ns
207 ns
9+
8+
16+
9+
275 ns

Figure 4

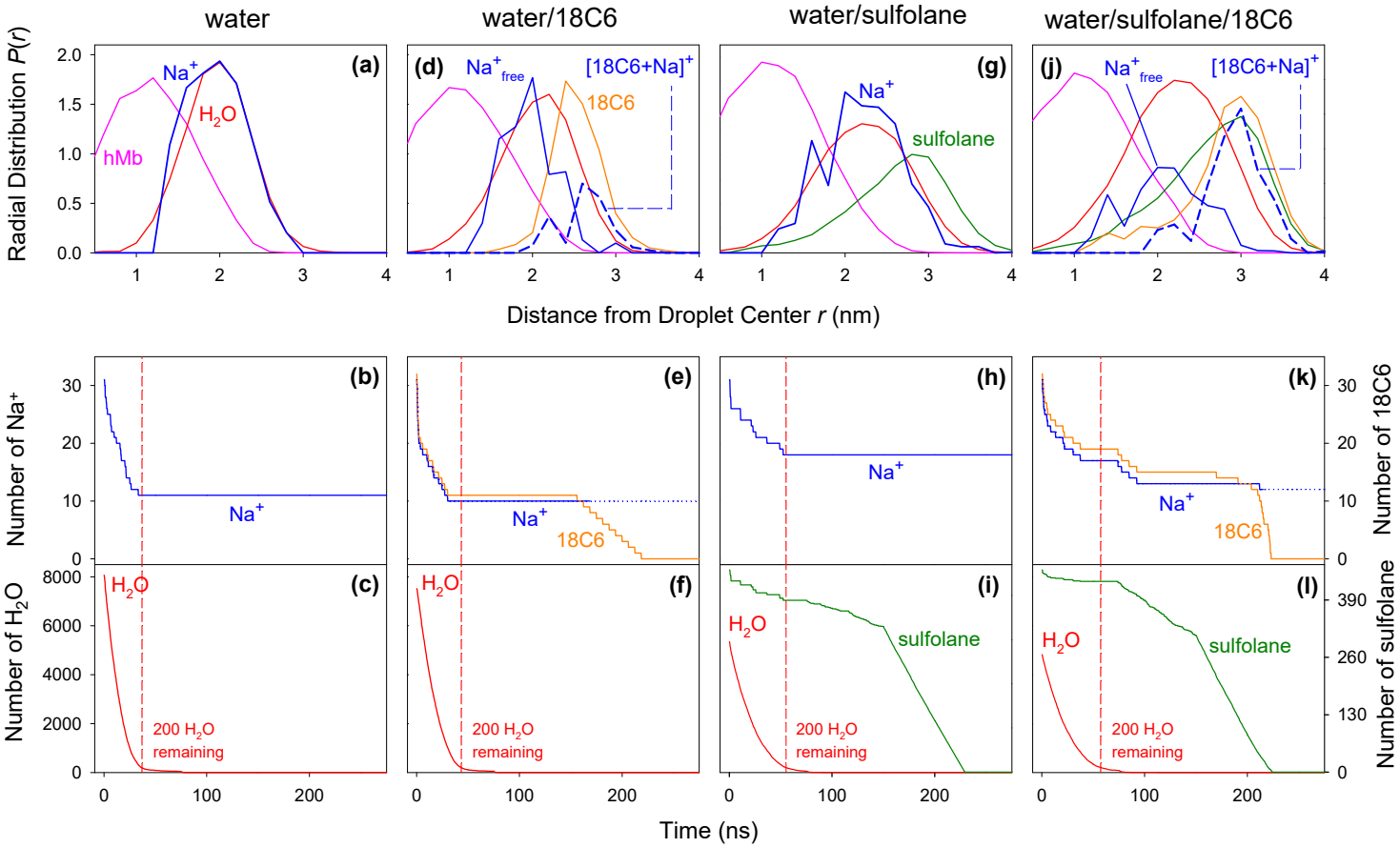
water
water/18C6
water/sulfolane
water/sulfolane/18C6
Radial Distribution P(r)
(a)
(d)
(g)
(j)
Na+
H2O
hMb
Na+free
[18C6+Na]+
18C6
sulfolane
Distance from Droplet Center r (nm)
(b)
(e)
(h)
(k)
(c)
(f)
(i)
(l)
Number of Na+
Number of H2O
Number of 18C6
Number of sulfolane
200 H2O remaining
Time (ns)

Figure 5

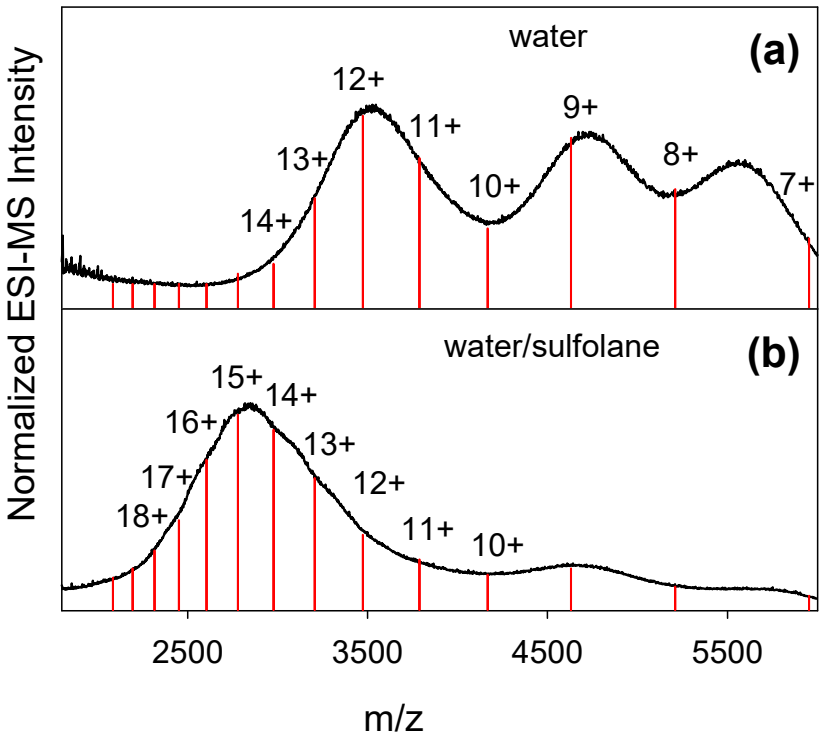
water
(a)
12+
11+
9+
13+
8+
10+
7+
14+
water/sulfolane
(b)
15+
14+
16+
13+
17+
12+
18+
11+
10+
Normalized ESI-MS Intensity
2500
3500
4500
5500
m/z

Figure 6

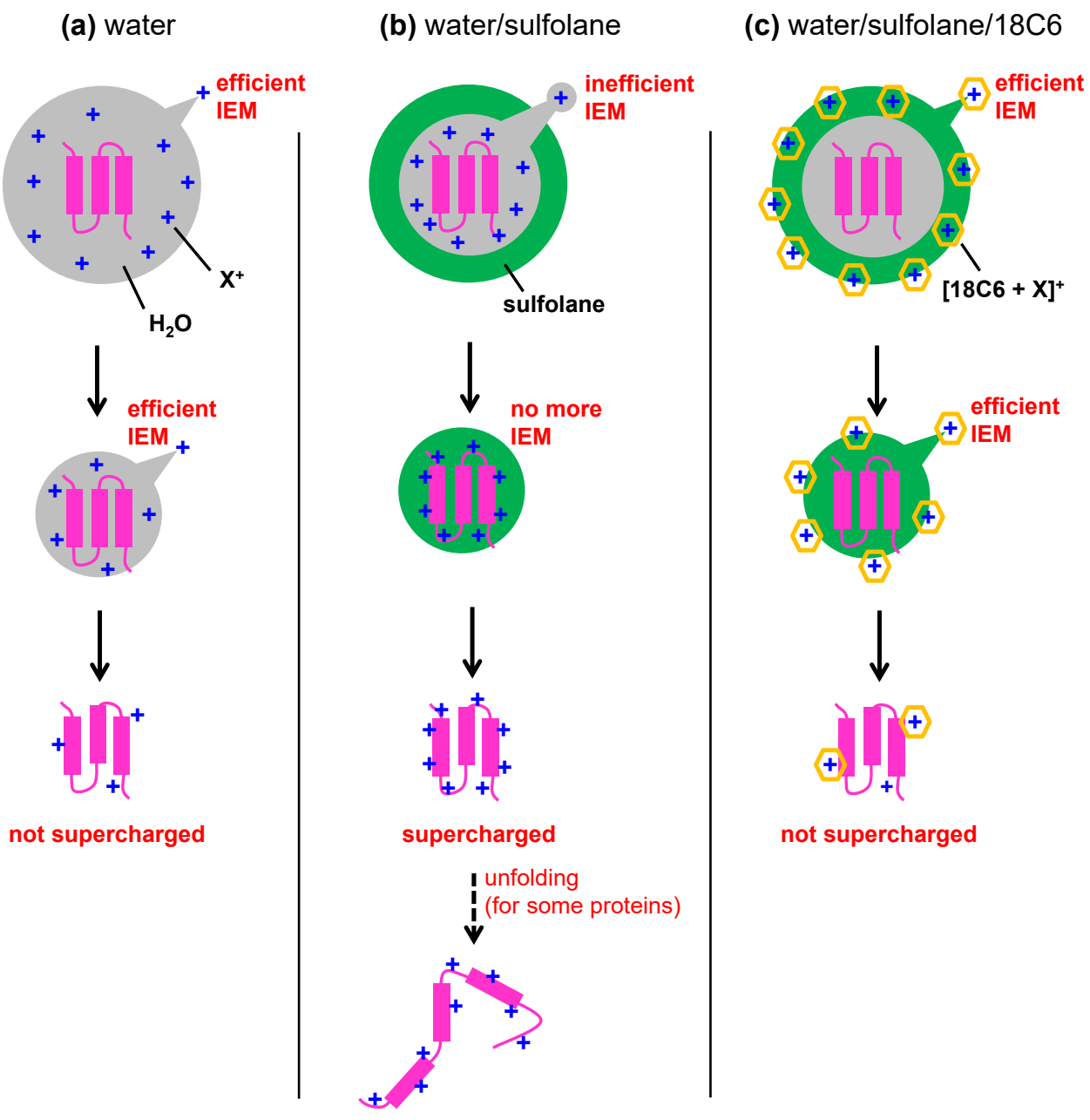
(a) water
efficient IEM
X+
H2O
efficient IEM
not supercharged
(b) water/sulfolane
inefficient IEM
sulfolane
no more IEM
supercharged
unfolding (for some proteins)
(c) water/sulfolane/18C6
efficient IEM
[18C6 + X]+
efficient IEM
not supercharged

For Table of Contents Only

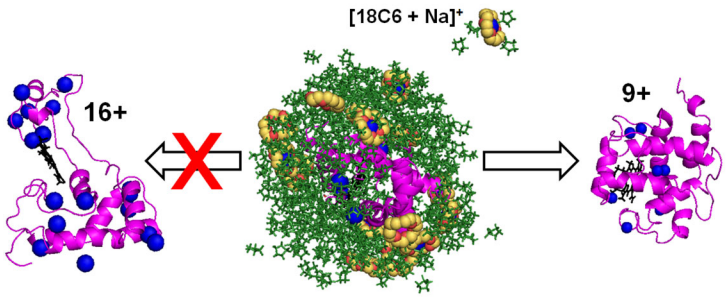

crown ether = ESI supercharging antidote